



# Effect of holmium oxide on impedance and dielectric behavior of polyaniline–holmium oxide composites

S. Manjunatha<sup>1,2</sup> · A. Sunilkumar<sup>1</sup> · Y. T. Ravikiran<sup>3</sup> · T. Machappa<sup>1</sup>

Received: 13 January 2019 / Accepted: 19 April 2019 / Published online: 29 April 2019  
© Springer Science+Business Media, LLC, part of Springer Nature 2019

## Abstract

Applying chemical in situ polymerization method, conducting polyaniline–holmium oxide (PANI/Ho<sub>2</sub>O<sub>3</sub>) composites with varying wt% of Ho<sub>2</sub>O<sub>3</sub> in PANI were prepared. Composites were characterized by Fourier-transform infrared spectroscopy, X-ray diffraction, Raman spectroscopy, thermogravimetric analysis, field emission scanning electron microscopy, energy dispersive X-ray spectroscopy and transmission electron microscopy. Room temperature frequency response conductivity and the dielectric studies of the as synthesized composites were investigated in the range 50 to 10<sup>6</sup> Hz. AC conductivity was found to decrease with the increasing wt% of Ho<sub>2</sub>O<sub>3</sub>. Further, conductivity of the composites obeyed power law of disordered materials. Cole–Cole plots for each composite, depicted single semicircle inferring that the conduction is due to the hopping of charge carriers. With increasing wt% of Ho<sub>2</sub>O<sub>3</sub>, dielectric constant and dielectric loss both decreased and at low frequencies, high dielectric constant of the composites, found decreasing with increasing applied frequencies due to Maxwell–Wagner type polarization. Tangent loss plots showed relaxation peaks at the resonant frequency.

## 1 Introduction

The discovery of conducting polymers was a turning point, for the dawn of novel polymer composites and their innovative studies leading to the various applications of technological importance [1]. Amongst all the intrinsic conducting polymers, polyaniline has dragged the dramatic attention due to its easy synthesis and processability, environmental stability and economic viability. PANI has been studied vigorously with the metals, metalloids, nonmetals [2] particularly with the inorganic metal oxides like Nb<sub>2</sub>O<sub>5</sub> [3], NiFe<sub>2</sub>O<sub>4</sub> [4], NaVO<sub>3</sub> [5], ZnWO<sub>4</sub> [6], MgCrO<sub>4</sub> [7], ZrO<sub>2</sub> [8], CdO [9], TiO<sub>2</sub>, Y<sub>2</sub>O<sub>3</sub> [10], ZnFe<sub>2</sub>O<sub>4</sub> [11] and BaTiO<sub>3</sub> [12] all these have gathered tremendous research inputs and were

able to throw light and help in providing new insights to the transport mechanism in these polymer composites. These hybrid materials, have found wide range of applications like capacitors, solar cells, electromagnetic interference shielding, polymer light emitting diodes, ink, paint, conductive adhesive, [13] and sensors [14]. Apart from these conducting polymer hybrids, polymer materials based on alignates, dendrimers, hierarchically porous polymer microspheres, have found applications in biodegradable food packaging [15], treatment of industrial effluents [16], sensors [17] etc.

Our previous studies, particularly PANI with the magnetic oxides [4] and transition metal dichalcogenides [18], have seen an appreciable enhancement in their AC conductivities and dielectric properties. These studies motivated us to undertake the further studies on novel PANI composites to explore their transport properties. Although aforementioned various metal oxides were studied with PANI, yet there is a limited study with the rare earth oxides. Further, to enhance the scope of PANI composites, we chose holmium oxide as the filling material in PANI with the intension of forming a novel composite and studying their interaction, through vivid spectroscopic and imaging techniques. Hence forth along with PANI, holmium oxide a rare earth compound with a wide band gap of 5.3 eV, is extensively used for many technological applications [19–22] was chosen for the present study. In this direction, this is the first ever attempt to

✉ Y. T. Ravikiran  
ytrcta@gmail.com

✉ T. Machappa  
machappat@rediffmail.com

<sup>1</sup> Department of Physics, VTU Research Centre, Ballari Institute of Technology & Management, Ballari 583104, India

<sup>2</sup> Department of Physics, Cambridge Institute of Technology, Bengaluru 560036, India

<sup>3</sup> Department of PG Studies & Research in Physics, Govt. Science College, Chitradurga 577501, India

study the ac conductivity and dielectric properties of the PANI/Ho<sub>2</sub>O<sub>3</sub> composite with varying wt% of Ho<sub>2</sub>O<sub>3</sub>, synthesized using in situ chemical polymerization method and characterized with Fourier-transform infrared spectroscopy (FTIR), X-ray diffraction (XRD), Raman spectroscopy, field emission scanning electron microscopy (FESEM), energy dispersive x-ray spectroscopy (EDX) and transmission electron microscopy (TEM) and thermal stability by thermogravimetric analysis (TGA). In order to get the more detailed information on the multifunctional device applications, its AC conductivity, impedance and the dielectric behavior of these composites were investigated at room temperature in the frequency range 50 to 10<sup>6</sup> Hz.

## 2 Experimental

### 2.1 Materials

Aniline (C<sub>6</sub>H<sub>5</sub>NH<sub>2</sub>) and hydrochloric acid (HCl) were procured from S.D. Fine Chemicals, Mumbai, India. Holmium oxide (Ho<sub>2</sub>O<sub>3</sub>) 99.99% from Aldrich. Aniline was double distilled prior to the synthesis of the composites. Throughout the synthesis of PANI and PANI/Ho<sub>2</sub>O<sub>3</sub> composites, distilled water was used.

### 2.2 Preparation of polyaniline and polyaniline–holmium oxide composites

PANI was synthesized applying in situ chemical polymerization method. Monomer aniline (2 mL) of 0.1 M was dissolved in 100 mL HCl of 1 M, along with stirring to form aniline hydroxide. Ammonium persulfate [(NH<sub>4</sub>)<sub>2</sub>S<sub>2</sub>O<sub>8</sub>] of 0.1 M, was mixed to the reaction mixture with continuous stirring for 6 h at a low temperature of 0 to 3 °C to polymerize into polyaniline. Precipitated product which was left behind, was filtered using vacuum and washed with distilled water. The product so obtained was dried in an oven for 1 day, to attain the constant weight of the polymer. Similarly, PANI–Ho<sub>2</sub>O<sub>3</sub> was synthesized under the same conditions but by adding finely grinded powder of Ho<sub>2</sub>O<sub>3</sub> with varying wt% like 10, 20, 30 and 40 separately to the above PANI yield, during the continuous stirring of the reaction mixture. These products were vacuum filtered, cleaned with distilled water and finally kept in oven for a day to gain the constant weight.

### 2.3 Characterization

XRD spectra of PANI, Ho<sub>2</sub>O<sub>3</sub> and PANI/Ho<sub>2</sub>O<sub>3</sub> composites were obtained in the range 2θ = 10° to 70° by powder X-ray diffractometer (Bruker D8 Advance, Cu Kα source, λ = 1.541 Å). FTIR spectra of the samples were obtained in the range 400–4000 cm<sup>-1</sup> by a FTIR Frontier PerkinElmer

instrument. Raman spectra in the range 200–2000 cm<sup>-1</sup> were obtained with a Horiba JobinYvonLabRam HR 800 Spectrometer (20 mW), using Ar laser (514.5 nm). FESEM images were captured with FEI Nova Nano SEM 600 instrument by loading the samples on an aluminium tape. TEM images were recorded using JEOL-3010 instrument operating at an accelerating voltage of 300 kV attached with a Gatan CCD camera. TGA was done using a Metler Toledo TGA-850 TG instrument at a heating rate of 5 °C/min from 30 to 800 °C under a nitrogen flow (40 mL/min).

## 2.4 AC Response measurements

At first the samples were ground for an hour. HCl doped PANI pellet and its Ho<sub>2</sub>O<sub>3</sub> composites pellets were prepared with diameter of 10 mm and thickness of 1 mm by pressing samples with a hydraulic pressure of around 4 tons. Frequency dependent AC response in the range 50–10<sup>6</sup> Hz, of the samples were investigated, programmable computer interfaced digital LCR meter (Japan) using a Hioki model 3532-50.

## 3 Results and discussion

### 3.1 FTIR Studies

Figure 1a represents FTIR absorption of PANI, with its typical bands at 1575 and 1487 cm<sup>-1</sup> representing C=C stretching vibrations of quinoid and benzenoid rings. The stripes at 1306, 1144, 858, 803 cm<sup>-1</sup> agree with C–N stretching, N=Q=N stretching (Q-quinoid), C–H out of plane stretching of the scented rings and C–H in plane stretching respectively. Also, the appearance of 1487 cm<sup>-1</sup> band and 1575 cm<sup>-1</sup> band with lesser absorption intensity together with a negligible broad absorption at 3233 cm<sup>-1</sup> all confirm the formation of PANI in emeraldine salt form [23]. Figure 1b depicts IR absorption spectrum of Ho<sub>2</sub>O<sub>3</sub>, which manifest its characteristics band at 554 cm<sup>-1</sup>, indeed its intense frequency band related to Ho–O vibrations, giving the evidence for metal–oxygen stretching on par with the literature [24]. Figure 1c convey the FTIR spectrum of the composite, the band at 1306 cm<sup>-1</sup> indicate decline in the absorption intensity of PANI in the composite, which is the confirmation of the integrated composite [25]. The recede from view of 3233 cm<sup>-1</sup> band of PANI in the composite specify non-existence of N–H stretching vibrations, and resulting in the strong interaction between PANI and Ho<sub>2</sub>O<sub>3</sub> [26]. This infers that the electron density of PANI chains has decreased in the composite, thereby leading to the decrease in its conductivity. Also, the band at 1144 cm<sup>-1</sup> is the charge delocalization band of the composite, comparatively has lesser absorption than that of the pristine PANI

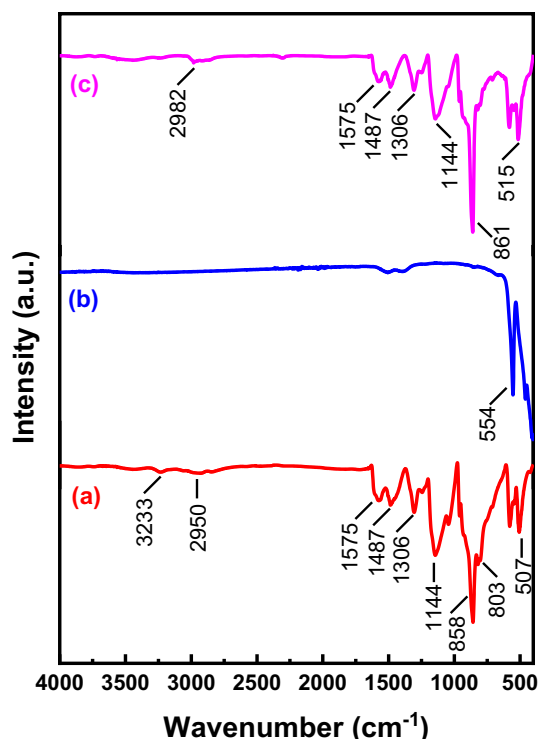
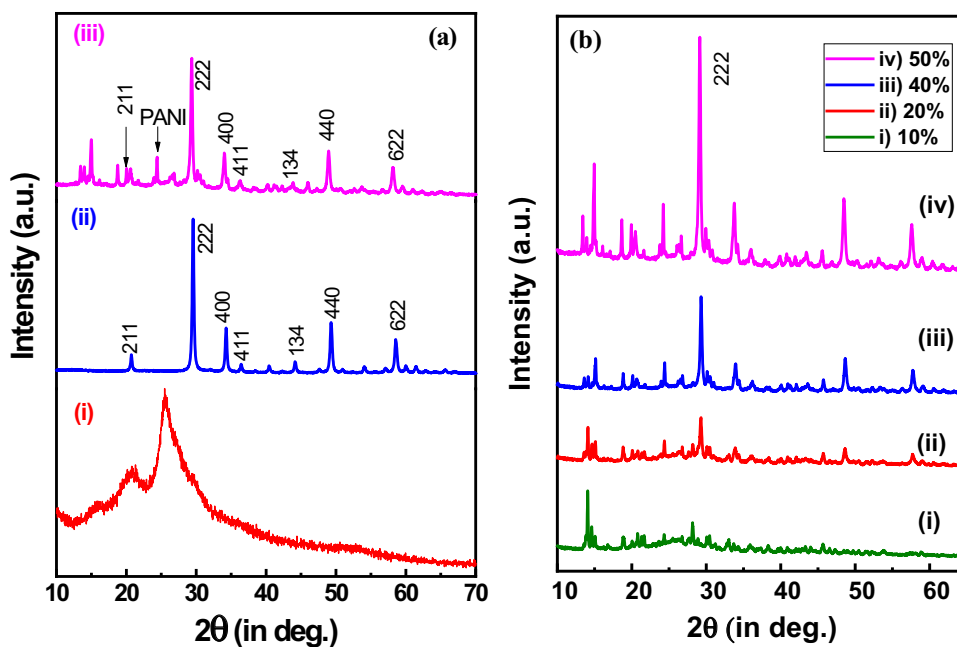


**Fig. 1** FTIR spectra of **a** pristine PANI, **b**  $\text{Ho}_2\text{O}_3$ , **c** PANI/ $\text{Ho}_2\text{O}_3$ -30%

inferring the decreased  $\pi$ - electron delocalization and the consequent decrease in conductivity can be realized [10]. Apart from these, the bands at 507, 580, 858  $\text{cm}^{-1}$  of PANI have shifted to 515, 582, 861  $\text{cm}^{-1}$  towards higher frequency sides in the composite, conclude the interfacial interaction between the polymer and the metal oxide [23].

**Fig. 2** XRD pattern of **a** (i) pristine PANI, (ii)  $\text{Ho}_2\text{O}_3$ , (iii) PANI/ $\text{Ho}_2\text{O}_3$ -30%, **b** XRD pattern of PANI/ $\text{Ho}_2\text{O}_3$  composites with different wt% of  $\text{Ho}_2\text{O}_3$



### 3.2 XRD Studies

Figure 2a(i) render the XRD pattern of PANI, clearly manifest two wide-range peaks at  $2\theta = 21.3^\circ$  and the outrageous peak at  $25.5^\circ$  which are associated with lattice periodicity in the direction parallel and perpendicular to the PANI polymer chains [4]. The alternative peaks of PANI illustrates the short range of chain ordering. Figure 2a(ii) convey diffraction pattern of  $\text{Ho}_2\text{O}_3$  offering the Bragg reflections in the extent of  $2\theta = 10\text{--}70^\circ$  which is tangible to the holmium oxide with a body-centered cubic (bcc) structure. The holmium oxide as illustrious C-type holmium sesquioxide with the bcc lattice parameter  $a = 10.6 \text{ \AA}$  belonging to Ia-3 space group [27]. Diverse Bragg reflections of  $\text{Ho}_2\text{O}_3$ , have presented its main peaks at  $2\theta \sim 20.7^\circ, 29.5^\circ, 34.3^\circ, 36.4^\circ, 44.1^\circ, 49.3^\circ, 58.5^\circ$  correlate with (211), (222), (400), (411), (134), (440) and (622) crystal planes respectively, which are in accordance with the Joint Committee on Powder Diffraction Standard (JCPDS) data file no. 65-3177. Figure 2a(iii) shows diffraction pattern of PANI/ $\text{Ho}_2\text{O}_3$ -30% composite synthesized from chemical polymerization method. The peaks of  $\text{Ho}_2\text{O}_3$  have come into view with an appreciable intensity, in which the composite has exhibited the same (222) crystal plane as the preferential orientation. Most of the peaks of the  $\text{Ho}_2\text{O}_3$  have appeared in the composite, retaining its crystalline phase and thus inferring that the oxide has been embedded in the matrix of PANI chains. It is noteworthy that, with the increase in wt% of  $\text{Ho}_2\text{O}_3$  in the composite, their crystallinity also increased in the preferential crystal direction (222) as that of  $\text{Ho}_2\text{O}_3$ , depicted in the Fig. 2b. This reveals the crystalline behavior of the composites. Also, the average crystallite size in the composite was

found to be around 50 nm as calculated by Debye-Scherrer's formula given in Eq. 1 and applied to the most intense peak at  $2\theta = 29^\circ$ .

$$\text{Crystallite size } t = \frac{k\lambda}{b \cos \theta} \quad (1)$$

where  $k$  is a constant taken to be 0.9,  $\lambda$ - wavelength of the X-rays used ( $\lambda = 1.541 \text{ \AA}$ ),  $b$ - is the full width at half maximum of the most intense peak of XRD pattern,  $2\theta$ - Bragg angle.

### 3.3 Raman spectra

Figure 3a shows the Raman spectra of PANI which represents its characteristics bands at  $1342$  and  $1590 \text{ cm}^{-1}$  for  $\text{C-N}^{+\cdot}$  as well as  $\text{C=C}$  stretching vibrations of quinoid rings respectively [28]. Figure 3b shows the defined Raman bands for C-type  $\text{Ho}_2\text{O}_3$  with the intense band observed at  $381 \text{ cm}^{-1}$  which is assigned as  $\text{A}_g + \text{T}_g$  mode, a consequent of the large change in polarizability during vibrations. Additionally, this most intense band is the characteristic Raman band for the rare earth sesquioxides of C-type in normal conditions [29–31]. The other observed modes such as  $319 \text{ cm}^{-1}$  has been assigned to  $\text{E}_g + \text{T}_g$  mode,  $335 \text{ cm}^{-1}$  corresponds to  $\text{E}_g$  mode,  $475 \text{ cm}^{-1}$  to  $\text{T}_g$ ,  $594 \text{ cm}^{-1}$  also corresponds to  $\text{T}_g$  mode. As per the factor group theory, twenty-two Raman modes have been estimated for the rare earth sesquioxides of C-type, but all the modes are not available in the literature. Figure 3c and d shows the Raman spectrum of the composites with 30 and 50 wt% of  $\text{Ho}_2\text{O}_3$  in which bands at  $1370$  and  $1555 \text{ cm}^{-1}$

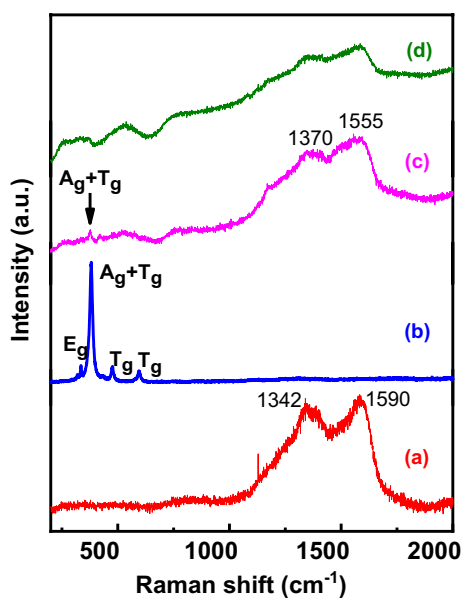


**Fig. 3** Raman spectra of **a** pristine PANI, **b**  $\text{Ho}_2\text{O}_3$ , **c** PANI/ $\text{Ho}_2\text{O}_3$ -30, **d** PANI/ $\text{Ho}_2\text{O}_3$ -50%

of PANI are observed significantly. The strong band corresponding to the  $\text{A}_g + \text{T}_g$  mode of  $\text{Ho}_2\text{O}_3$  was suppressed with a shift in bands corresponding to PANI indicating the strong interaction between them. All the other modes of the rare earth oxide were greatly suppressed and hardly can be seen in the composites.

### 3.4 TGA Studies

Figure 4a represents thermic mortification of pristine PANI which has shown a quality type of behavior indicating deprivation in three dissimilar steps [18]. Deprivation at  $110^\circ\text{C}$ , may hold responsible for the ejection of water molecules present in PANI. The next deprivation is observed at net positive charges of PANI chains at  $220^\circ\text{C}$ , associated with characteristic loss of  $\text{Cl}^-$  dopant anions, last deprivation at  $300^\circ\text{C}$  may be due to the thermal deterioration of PANI chains resulting in the loss of dopant ions. Altogether reduction of 65% weight of PANI has been observed in the temperature range of 30 to  $800^\circ\text{C}$ . Figure 4b shows of about 53% weight loss of PANI/ $\text{Ho}_2\text{O}_3$ -10% composite which is observed according to a particular sequence. Figure 4c and d shows PANI/ $\text{Ho}_2\text{O}_3$ -30% and 50 wt% respectively, which are in the neighborhood illustrating the weight loss as good as PANI with 45 and 42% respectively. Whereas bulk  $\text{Ho}_2\text{O}_3$  as in Fig. 4e, exhibited a negligible weight loss of less than 1% till  $800^\circ\text{C}$ . This may be due to the expulsion of water molecules/moisture. The composites were found to be more stable thermally by exhibiting a lower rate of weight loss at all the temperatures in the measured range as compared to that of pristine PANI.

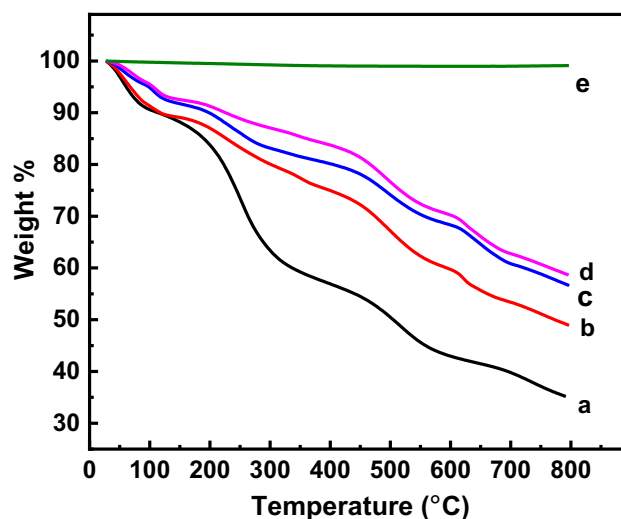


**Fig. 4** TGA curves of **a** PANI, **b** PANI/ $\text{Ho}_2\text{O}_3$ -10%, **c** PANI/ $\text{Ho}_2\text{O}_3$ -30%, **d** PANI/ $\text{Ho}_2\text{O}_3$ -50%, **e**  $\text{Ho}_2\text{O}_3$

### 3.5 FESEM and EDX studies

Figure 5 shows the FESEM and EDX images of the sample. Figure 5a reveals the monotonous distribution of granulated structures of less than 1  $\mu\text{m}$  observed in pristine PANI. Figure 5b shows as procured ungrounded  $\text{Ho}_2\text{O}_3$  particles, in the form of wafer like structures of size around 1–5  $\mu\text{m}$ . Figure 5c depicts morphology of the PANI/ $\text{Ho}_2\text{O}_3$ -30% composite, wherein agglomerated structures with uneven surfaces of sizes in the range 1–5  $\mu\text{m}$  were found. This kind of agglomerated structures which are not densely packed, compared to that of pristine PANI, implying the increase in inter-granular distance between the grains in the composite and thereby leading to the decrease in conductivity of the composite [14]. Such morphology is very much conducive for gas and humidity sensing applications. This kind of morphological structures has been reported in the recent literature [18]. Figure 5d shows (EDX) Energy dispersive X-ray spectrum, exhibiting the peaks of carbon, nitrogen and chlorine from PANI as well as holmium and oxygen peaks from holmium oxide in the appropriate ratio. Thus, these peaks manifest the formation of the composite and the elemental composition is in close agreement with that of the composition taken during the synthesis of the composite

PANI/ $\text{Ho}_2\text{O}_3$ -30 wt%. The details of the elemental composition obtained by EDX is given in Table 1.

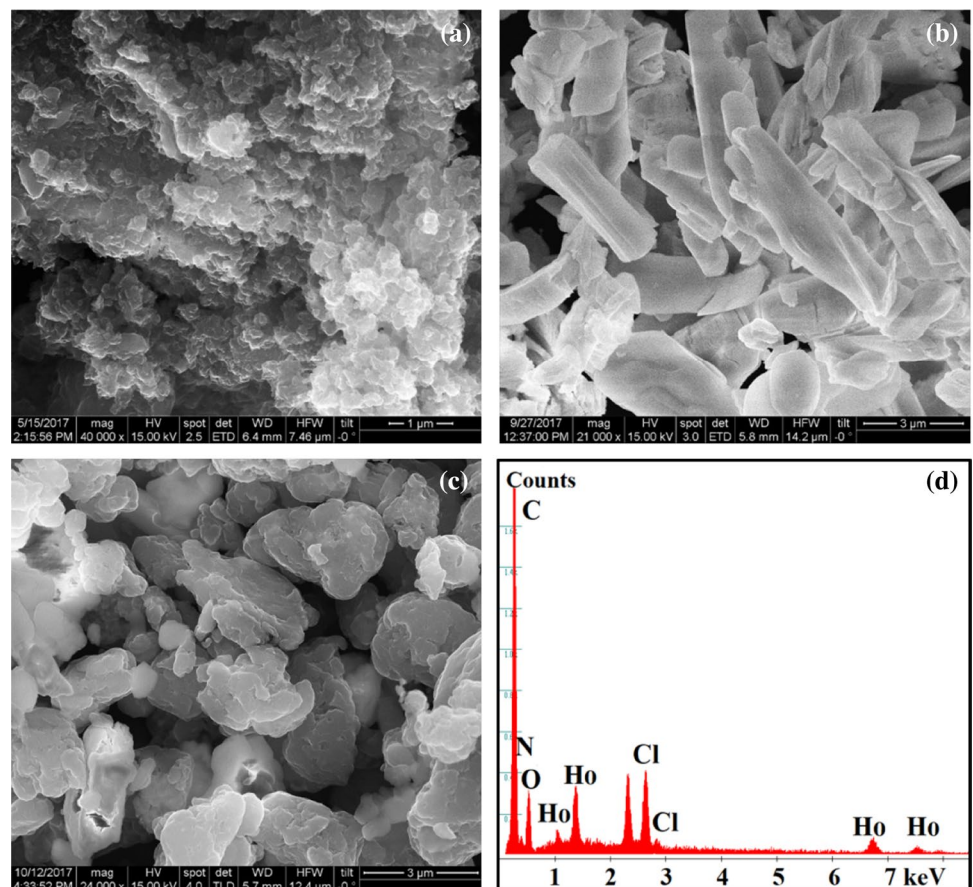
### 3.6 TEM studies

TEM image, SAED pattern and HRTEM image of PANI/ $\text{Ho}_2\text{O}_3$ -40% composite are shown in Fig. 6. Morphological structure of the composite has unraveled a kind of encapsulated structure, wherein the denser rare earth metal oxide particles, are seen as the dark central region in Fig. 6a. These oxide particles have been wrapped by the lighter organic PANI matrix. The size distribution of these structures is in good agreement with those of the structures found in FESEM studies. During the synthesis of the PANI-metal oxide composites by the in situ chemical polymerization

**Table 1** Elemental composition of PANI/ $\text{Ho}_2\text{O}_3$ -30% composite as obtained by EDX

Element	Energy (keV)	wt%
C	0.27	65.67
N	0.39	4.4
O	0.52	7.29
Cl	2.62	6.21
Ho	1.35	16.43

**Fig. 5** Field emission scanning electron micrographs of **a** HCl doped PANI **b**  $\text{Ho}_2\text{O}_3$  **c** PANI/ $\text{Ho}_2\text{O}_3$ -30% **d** EDX spectrum of PANI/ $\text{Ho}_2\text{O}_3$ -30% composite



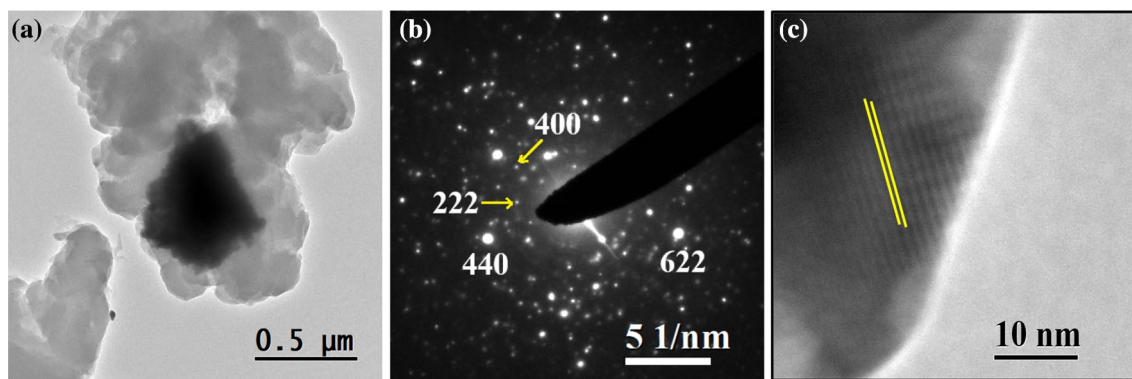


**Fig. 6** a TEM b SAED pattern c HRTEM image of PANI/Ho<sub>2</sub>O<sub>3</sub>-40% composite

technique, the formation of such encapsulated structures is common and has been reported in the literature [18]. Also, the SAED pattern exhibits the diffraction spots confirming the crystalline nature of the encapsulated structures, which has been already revealed by XRD characterization. Different lattice planes have been identified in the SAED pattern by using Au standard method as shown in Fig. 6b. HRTEM image captured at the edge of the interfacial region of the composite show lattice fringes as depicted in Fig. 6c. Such crystalline structures as revealed by the SAED and XRD pattern are highly useful in chemi-resistive sensors.

### 3.7 AC Conductivity

AC conductivity in disordered materials is given by  $\sigma(f) = \sigma'(f) - i\sigma''(f)$ , where  $\sigma'(f)$  is the real part and  $\sigma''(f)$  constitutes the imaginary part of the conductivity. General behavior of the real part of conductivity  $\sigma'(f)$  in disordered materials takes the form

$$\sigma'(f) \approx \sigma'(0), \text{ when } f < f_c \quad (2)$$

$$\sigma'(f) \propto f^s, \text{ when } f > f_c \quad (3)$$

At low frequencies, conductivity  $\sigma'$  is unvarying and independent of the applied AC frequency, which can be realized to the DC conductivity  $\sigma'(0)$ . But at higher applied frequencies, conductivity  $\sigma'$  rises with the applied frequency of the field. This high frequency regime can be approximated using a power law as given in Eq. 3, with the exponent  $s$ , value lying in between 0 and 1 or equal to 1. The transition from the frequency independent regime to the frequency dependent regime can be marked by a frequency  $f_c$  called as critical frequency. Hence, AC conductivity in the disordered materials can be given by

$$\sigma = \sigma'_{dc} + \sigma'_{ac} \quad (4)$$

$\sigma'_{dc} = \sigma'(0)$  is the DC conductivity which is usually featured by the models, where hopping of electrons near the

Fermi energy is considered, such as Mott model of conductivity and  $\sigma'_{ac}$  is the conductivity due to the frequency dependent regime above the critical frequency [32].

Frequency dependent electrical conductivities of PANI/Ho<sub>2</sub>O<sub>3</sub> composites are shown in the Fig. 7. Initially conductivity of the composites was observed to be sustained, till the frequency gets as far as critical frequency. Above the critical frequency conductivity began to increase, which is in well agreement with the earlier literatures [3]. One of the most important observations is that, the conductivity of all the composites is considerably lower than that of pristine PANI, in spite of the fact that holmium oxide is rare earth oxide with wide band gap insulating material. Conductivity of the pristine PANI was found to be  $10^{-4} \text{ Scm}^{-1}$  which is on par with the reported literature [18]. As we increase the wt% of Ho<sub>2</sub>O<sub>3</sub> in the PANI composites, the conductivity was found to

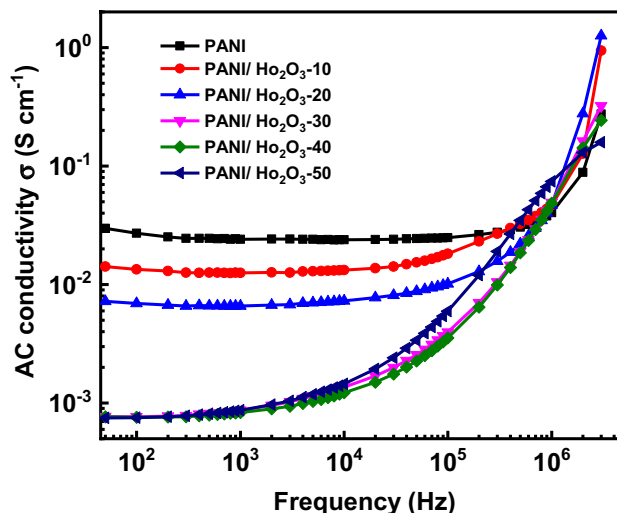


**Fig. 7** Variation of AC conductivity as function of frequency for HCl doped pristine PANI and its composites with 10, 20, 30, 40 and 50 wt% of Ho<sub>2</sub>O<sub>3</sub>

decrease drastically. Critical frequency  $f_c$  was also found to decrease with increasing wt% of  $\text{Ho}_2\text{O}_3$  from 200 kHz for 10 wt% to 10 kHz for the 50 wt% composite, which are tabulated in Table 2, for all the composites. This decrease in  $f_c$  is as expected, which is generally known to decrease with the conductivity.

Conductivity of the composites depends on vivid reasons like extent of protonation, crystallinity, size and order of arrangement of crystalline domains in the matrix of the amorphous PANI. Initially for 10 and 20 wt% composites the conductivity was found to decrease by one order, due to the fact that distribution of holmium oxide, might have hindered the hopping of charge carriers and resulted in the decrease of conductivity. Whereas for 30, 40 and 50 wt% of  $\text{Ho}_2\text{O}_3$  in the composites, exhibited higher order of decrease in conductivity as compared to that of pristine PANI. The increased wt% of holmium oxide in PANI composites probably led to depletion in delocalization length and the consequent higher order decrease in its conductivity was observed than the pristine PANI.

### 3.8 Impedance spectroscopy

The impedance plots of PANI and the composites are depicted in Fig. 8. Cole–Cole plot of pristine PANI shown in Fig. 8a, exhibited a semicircle and the relaxation mechanism is of Debye-type as expected [18]. Interestingly, the impedance plots of PANI/ $\text{Ho}_2\text{O}_3$  composites have also exhibited semicircles and the relaxation follows Debye model as shown in Fig. 8a. Area under each semicircle of the spectrum of the composites was found to be increasing with increasing wt% of  $\text{Ho}_2\text{O}_3$ , indicating the decrease in corresponding conductivities starting from pristine PANI. At the outset, area under the curves were found increasing compared to PANI, in the ascending order of 10, 20, 30, 40 and 50 wt% composites, inferring the massive decrease of conductivities. Relaxation time for pristine PANI from the impedance plot was found to be 1.523  $\mu\text{s}$  which is in good agreement with the earlier literature [3]. It can also be observed that for 30 and 40 wt% composites, critical frequency was found to be 20 kHz and the area under these curves are more or less same, exhibiting same relaxation time of 53.05  $\mu\text{s}$ , as calculated by the relation  $\tau = 1/(2\pi f_p)$ ,

**Table 2** Summary of AC electrical response of PANI/ $\text{Ho}_2\text{O}_3$  composites

Sample	AC conductivity at 20 kHz ( $\sigma'$ S cm <sup>-1</sup> )	Power law index (s)	Critical frequency ( $f_c$ kHz)	Relaxation time ( $\tau$ $\mu\text{s}$ )	Frequencies at the relaxation peaks ( $f_p$ kHz)	Dielectric constant at 100 Hz ( $\epsilon'$ )	Dielectric loss at 1000 Hz ( $\tan \theta$ )
HCl doped PANI	$2.39 \times 10^{-4}$	0.69	500	1.52	300	$2.28 \times 10^5$	2685.5
PANI/ $\text{Ho}_2\text{O}_3$ -10%	$1.37 \times 10^{-4}$	0.51	200	2.65	60	$5.21 \times 10^4$	35.6
PANI/ $\text{Ho}_2\text{O}_3$ -20%	$7.74 \times 10^{-6}$	0.66	100	5.30	30	$1.69 \times 10^4$	13.5
PANI/ $\text{Ho}_2\text{O}_3$ -30%	$1.69 \times 10^{-6}$	0.68	20	53.05	3	$9.21 \times 10^3$	2.6
PANI/ $\text{Ho}_2\text{O}_3$ -40%	$1.49 \times 10^{-6}$	0.69	20	53.05	3	$5.84 \times 10^3$	3.2
PANI/ $\text{Ho}_2\text{O}_3$ -50%	$1.93 \times 10^{-6}$	0.73	10	79.57	2	$1.09 \times 10^4$	2.2

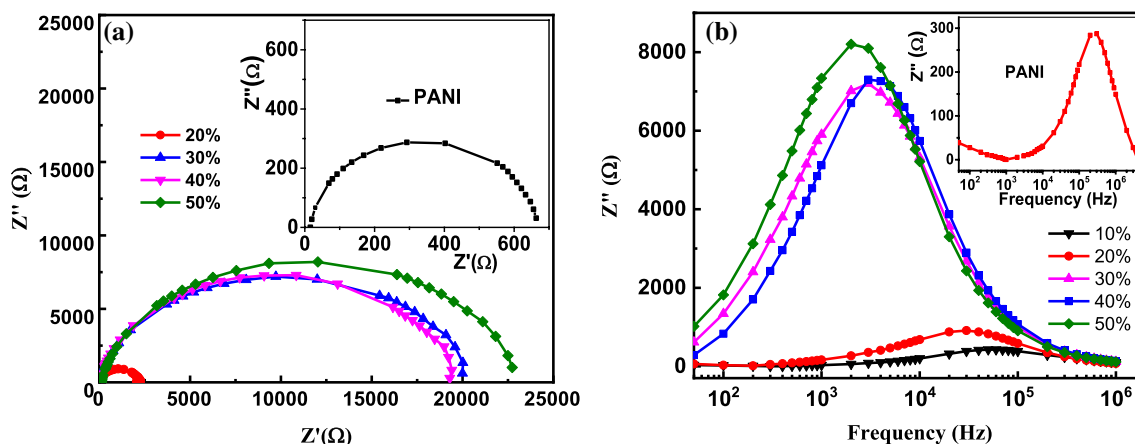


**Fig. 8** **a** Complex impedance plots for PANI/ $\text{Ho}_2\text{O}_3$  composites, inset: for pristine PANI, **b** Nyquist plots of the composites, inset: for pristine PANI

where  $f_p$ - frequency corresponding to the peak position of the impedance plot for the respective wt% composition. Relaxation times for all the composites have been given in Table 2. The minute digression from an ideal semicircle can be considered to be heterogeneous distribution of holmium oxide throughout the sample specifying relaxation follows nearly Debye-type which is in good confirmation with the earlier studies. The complex impedance plots of single deprived semicircle, show the absence of diffusion of ions at the electrodes this may be responsible for uncharged ions found in the composites. Single semicircle of the Cole–Cole plot, indicate that the equivalent circuit can be visualized to be made of resistance and capacitor in parallel combination. This type of electrical circuit, according to Dyre, can be correlated to an amorphous semiconductor and the conductivity would be due to hopping of charge carriers [33]. Further, the absence of any kind of spikes in the impedance plots indicate that the conductivity in the material is solely due to electrons and rules out the possibility of conduction due to diffusion of ions [34].

As the wt% of  $\text{Ho}_2\text{O}_3$  increases in the composites, the relaxation frequency shifts towards the lower side. The same can be realized by plotting imaginary part of the impedance versus applied frequencies, which are typically called Nyquist plots as shown in Fig. 8b. Inset of Fig. 8b is the plot of pristine PANI, exhibiting the relaxation peak at 300 kHz. Whereas, for the composites; it's quite interesting that the relaxation frequencies were 60, 30, 3, 3 and 2 kHz respectively for 10, 20, 30, 40 and 50 wt% samples as exhibited in Fig. 8b. These plots hint the bulk relaxation dynamics of the material and the single peak of each plot, infers that the relaxation is of single type. Among all the composites, conductivity of 10 wt% sample exhibited comparatively higher conductivity due to its fastest relaxation, which is of 2.65  $\mu\text{s}$ . As the relaxation phenomena can be correlated to the charge transport through hopping mechanism, increased relaxation times can be realized with the rise in hopping length, due to the stretching effects of  $\text{Ho}_2\text{O}_3$  and thereby providing explanation for the decreased values of the conductivities of the composites [3].

### 3.9 Dielectric studies

Dielectric constant and tangent loss were studied as a function of frequency for all the composites. Figure 9 illustrates the variation of dielectric constant with the applied AC frequencies for PANI/ $\text{Ho}_2\text{O}_3$  composites. At the low applied AC frequencies, dielectric constant was very high of around  $10^6$  order. As the applied frequency of the field increases, dielectric constant decreases gradually, indicating the normal dielectric behavior of the conducting polymer composites, which is on par with our recent studies [18]. Higher values of permittivity at lower frequencies may be attributed

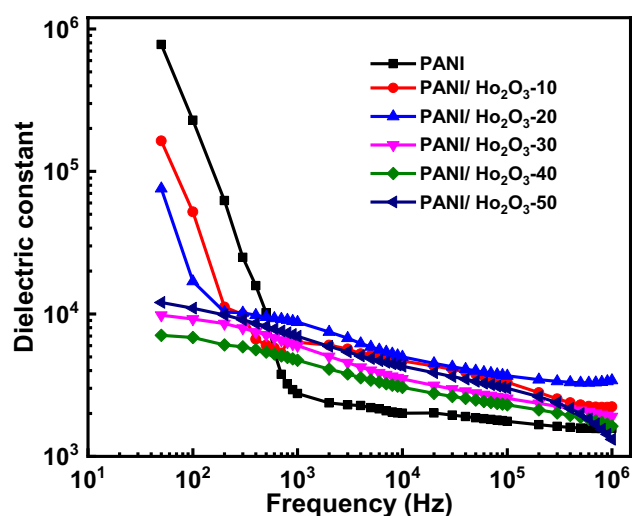
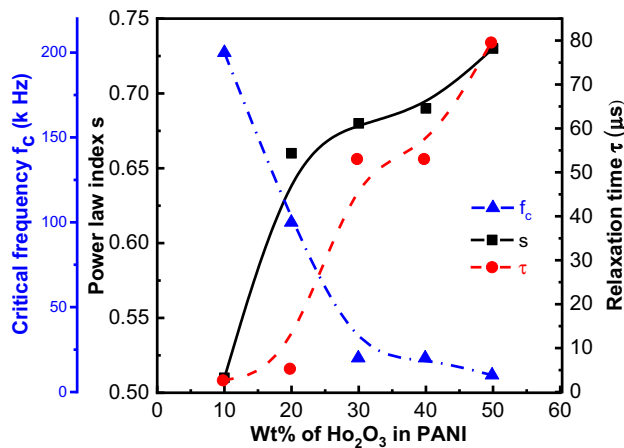


Fig. 9 Variation of dielectric constant as a function of applied frequency for pristine PANI and the PANI/ $\text{Ho}_2\text{O}_3$  composites

to the electrode polarization and space charge polarization effects [35]. Dielectric constant of pristine PANI is observed to be  $2.2 \times 10^5$  at 100 Hz and 161 at 1 kHz. Decrease in dielectric constant with increasing frequencies can be elucidated by Maxwell–Wagner polarization model [36]. Variation of dielectric constant with the applied frequencies can be explained on the basis of hopping frequency of the charge carriers. Since the hopping frequency of the charge carriers follows frequency of the applied field, which results in higher values of dielectric constant. On the other hand, at higher frequencies, hopping frequency lags behind the applied frequency of the AC field, which results in dielectric constant of lower values because of the random dipolar orientation [37]. Also, the dielectric constant found decreasing, with the increasing wt% of  $\text{Ho}_2\text{O}_3$  in the composites. For 10 and 20 wt% composites dielectric constant decreased in a specific range, whereas for 30, 40 and 50 wt% composites, dielectric constant decreased ambiguously. Also, values of the dielectric constant for 10 and 50 wt% composites at 100 Hz were observed at  $5.21 \times 10^4$  and  $1.09 \times 10^4$  respectively. For all other composites, dielectric constant at 100 Hz has been tabulated in Table 2. It is worth to be noted that with the increase in wt% of  $\text{Ho}_2\text{O}_3$ , the values of dielectric constant at a particular frequency found to decrease. Using equations related to ac conductivity in disordered media as reported in our recent article [18], various AC parameters have been calculated and summarized in Table 2 and also depicted graphically in Fig. 10.

Variation of loss  $\tan \theta$  (dissipation factor) with the applied AC frequency of the composites is as shown in Fig. 11. Because of the dielectric relaxation peaks, all the composites exhibited abnormal dielectric behavior. Using Relescu model, formation of the dielectric relaxation peaks can be





**Fig. 10** Variation of critical frequency, power law index and relaxation time with wt% of  $\text{Ho}_2\text{O}_3$  in PANI

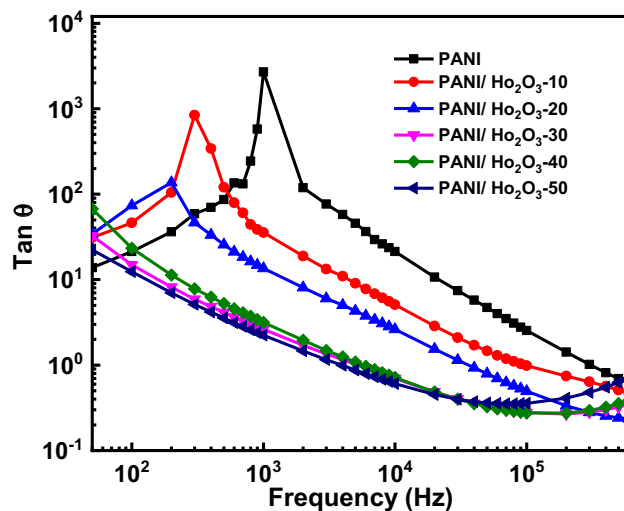


**Fig. 11** variation of  $\tan \theta$  as a function of frequency for pristine PANI and PANI/ $\text{Ho}_2\text{O}_3$  composites

explained [38]. Also, this type of typical dielectric behavior can also be explained by the development of small polarons leading to the charge polarization [39]. These dielectric relaxation peaks form, when hopping frequency of the localized charge carriers resonates with the externally applied AC frequencies [40]. Further, the value of  $\tan \theta$  is large at lower frequencies which represent the relaxation peaks. PANI exhibited the dielectric loss peak at 1000 Hz with a loss of  $2.6 \times 10^3$ . Similarly, among all the PANI/ $\text{Ho}_2\text{O}_3$  composites, 10 and 20 wt% composites exhibited the loss peaks within 1000 Hz. In summary, the values of  $\tan \theta$  were found to decrease with the increasing wt% of  $\text{Ho}_2\text{O}_3$  in the composites. Higher values of  $\tan \theta$  at the lower frequencies, may be helpful in designing the medium frequency devices.

Thus, the fall in dielectric constant and the conductivity with the applied frequency, infers that the higher values of dielectric constant are due to the conduction relaxation as discussed earlier. High dielectric loss at the lower frequencies in all the composites may be correlated to the losses due to DC conduction. Real part of ac conductivity, dielectric constant and the dielectric loss all exhibited the decreasing trend in the low frequency region, with the increase in wt% of  $\text{Ho}_2\text{O}_3$ . This behavior indicates the role of conduction charge carriers in dielectric response. Thus, the obtained results have gained significance with those of the trends observed in decrease in temperature or with the decrease in doping level.

## 4 Conclusion

PANI/ $\text{Ho}_2\text{O}_3$  composites were prepared by in situ polymerization method. Conductivity and dielectric studies of the composites exhibited the systematic AC response and dielectric behavior. Conductivity measurements revealed that the composites followed power law well above the critical frequency. Fall in conductivity with the rise in wt% of  $\text{Ho}_2\text{O}_3$  can be correlated to the conformational changes in the polymer matrix as well as their chain arrangements. Impedance spectra revealed that the relaxation is of Debye-type. At the low frequency region, the decrease in conductivity, dielectric constant and the tangent loss all found decreasing with the applied frequency as well as with the increase in wt% of  $\text{Ho}_2\text{O}_3$ . These variations in conductivity and dielectric properties can be correlated with those of the decrease in temperature and decrease in doping level. Because of the high dielectric losses at the low frequency regime and the presence of loss tangent peaks, these composites can be used for the device applications in the medium frequency range.

**Acknowledgements** Authors acknowledge Jawaharlal Nehru Centre for Advanced Scientific Research (JNCASR) Bengaluru, in providing facilities for structural characterization of the samples. S. Manjunatha thanks Sri D. K. Mohan, Chairman, Dr. L. Suresh, Principal, Cambridge Institute of Technology, Bengaluru for their support in research activity. All the authors render special thanks to Dr. Yashvanth Bhupal, Director and Prof. Y.J. Prithviraj, Dep. Director, Ballari Institute of Technology & Management, Ballari for their encouragement.

## References

1. T.K. Das, S. Prusty, *Polym. Plast. Technol. Eng.* **51**, 1487 (2012)
2. G. Ćirić-Marjanovic, *Synth. Met.* **170**, 31 (2013)
3. Y.T. Ravikiran, M.T. Lagare, M. Sairam, N.N. Mallikarjuna, B. Sreedhar, S. Manohar, A.G. MacDiarmid, T.M. Aminabhavi, *Synth. Met.* **156**, 1139 (2006)
4. R. Megha, Y.T. Ravikiran, S.C. Vijaya Kumari, S. Thomas, *Appl. Phys. A* **123**, 245 (2017)

5. T. Machappa, M.V.N.A. Prasad, *Phys. B Condens. Matter* **404**, 4168 (2009)
6. T. Machappa, M.V.N.A. Prasad, *Ferroelectrics* **392**, 71 (2009)
7. T. Machappa, S. Manjunatha, A. Sunilkumar, *Int. J. Sci. Technol. Manag.* **04**, 714 (2015)
8. B.P. Prasanna, D.N. Avadhani, H.B. Muralidhara, K. Chaitra, V.R. Thomas, M. Revanasiddappa, N. Kathyayini, *Bull. Mater. Sci.* **39**, 667 (2016)
9. M.V.N.A. Prasad, A.S. Roy, K.R. Anilkumar, *J. Appl. Polym. Sci.* **123**, 1928 (2012)
10. R. Megha, Y.T. Ravikiran, S.C. Vijaya Kumari, T. Chandrasekhar, S. Thomas, *Polym. Compos.* **39**, 3545 (2018)
11. R.D. Balikile, A.S. Roy, S.C. Nagaraju, G. Ramgopal, *J. Mater. Sci.* **28**, 7368 (2017)
12. P. Somani, B.B. Kale, D.P. Amalnerkar, *Synth. Met.* **106**, 53 (1999)
13. G. Ciric Marjanovic, *Synth. Met.* **177**, 1 (2013)
14. S. Manjunatha, T. Machappa, Y.T. Ravikiran, B. Chethan, A. Sunilkumar, *Phys. B Phys. Condens. Matter* **561**, 170 (2019)
15. J. Li, J. Ma, S. Chen, J. He, Y. Huang, *Food Hydrocoll.* **82**, 363 (2018)
16. M. Ma, Y. Yang, W. Li, R. Feng, Z. Li, P. Lyu, Y. Ma, *J. Mater. Sci.* **54**, 323 (2019)
17. K. Jiang, H. Zhao, J. Dai, D. Kuang, T. Fei, T. Zhang, *A.C.S. Appl. Mater. Interfaces* **8**, 25529 (2016)
18. S. Manjunatha, T. Machappa, A. Sunilkumar, Y.T. Ravikiran, *J. Mater. Sci.* **29**, 11581 (2018)
19. B. Karmakar, K. Annapurna, *J. Non. Cryst. Solids* **353**, 1377 (2007)
20. H.M. Shiri, A. Ehsani, *Bull. Chem. Soc. Japan* **89**, 1201 (2016)
21. T. Pan, M. Huang, *Mater. Chem. Phys.* **129**, 919 (2011)
22. S. Mortazavi-Derazkola, S. Zinatloo-Ajabshir, S.-N. Masoud, *J. Mater. Sci.* **28**, 1914 (2017)
23. R. Megha, Y.T. Ravikiran, S.C.V. Kumari, H.G.R. Prakash, CH.V.V. Ramana, S. Thomas, *Compos. Interfaces* **26**, 309 (2019)
24. S. Mortazavi-Derazkola, S. Zinatloo-Ajabshir, M. Salavati-Niasari, *Ceram. Int.* **41**, 9593 (2015)
25. V. Gautam, A. Srivastava, K.P. Singh, V.L. Yadav, *Polym. Sci. Ser. A* **58**, 206 (2016)
26. B.K. Sharma, N. Khare, S.K. Dhawan, H.C. Gupta, *J. Alloys Compd.* **477**, 370 (2009)
27. M.N. Abdusalyamova, F.A. Makhmudov, E.N. Shairmardanov, I.D. Kovalev, P.V. Fursikov, I.I. Khodos, Y.M. Shulga, *J. Alloys Compd.* **601**, 31 (2014)
28. Y.G. Wang, H.Q. Li, Y.Y. Xia, *Adv. Mater.* **18**, 2619 (2006)
29. G. Schaack, J.A. Koningstein, *J. Opt. Soc. Am.* **60**, 1110 (1970)
30. N. Dilawar, S. Mehrotra, D. Varandani, B.V. Kumaraswamy, S.K. Haldar, A.K. Bandyopadhyay, *Mater. Charact.* **59**, 462 (2008)
31. S.D. Pandey, K. Samanta, J. Singh, N.D. Sharma, A.K. Bandyopadhyay, *J. Appl. Phys.* **116**, 133504 (2014)
32. J. Bisquert, G.G. Belmonte, *Russ. J. Electrochem.* **40**, 352 (2004)
33. J.C. Dyre, *J. Appl. Phys.* **64**, 2456 (1988)
34. N. Maity, A. Kuila, S. Das, D. Mandal, A. Shit, A.K. Nandi, *J. Mater. Chem. A* **3**, 20736 (2015)
35. H.M. Kim, C.Y. Lee, J. Joo, *Korean Phys. Soc.* **36**, 371 (2000)
36. K.W. Wagner, *Ann. Phys.* **5**, 817 (1913)
37. A.K.M.S. Sinha, S.K. Chatterjee, J. Ghosh, *Polym. Compos.* **38**, 287 (2017)
38. N. Rezlescu, E. Rezlescu, *Phys. Status Solidi* **23**, 575 (1974)
39. J. Bao, J. Zhou, Z. Yue, L. Li, Z. Gui, *J. Magn. Magn. Mater.* **250**, 131 (2002)
40. I. Sadiq, S. Naseem, M. Naeem Ashiq, M.A. Khan, S. Niaz, M.U. Rana, *Prog. Nat. Sci. Mater. Int.* **25**, 419 (2015)

**Publisher's Note** Springer Nature remains neutral with regard to jurisdictional claims in published maps and institutional affiliations.